

Supporting Information

A Two-Electron Silver Superatom Isolated from Thermally Induced Internal Redox Reaction of A Silver(I) Hydride

Yu-Jie Zhong, Jian-Hong Liao, Tzu-Hao Chiu, Samia Kahlal, Che-Jen Lin, Jean-Yves Saillard, and C. W. Liu**

anie_202100965_sm_miscellaneous_information.pdf

Supplementary Information

Experimental Section

Materials and measurements

All chemicals were purchased from commercial sources and used as received. Solvents were purified following standard protocols.^{S1} All reactions were performed in oven-dried Schlenk glassware using standard inert atmosphere techniques. All reactions were carried out under N₂ atmosphere by using standard Schlenk techniques. Ag₇(H){S₂P(O^{*i*}Pr)₂}₆^{S2} and Ag₆{S₂P(O^{*i*}Pr)₂}₆^{S3} were prepared by a slightly modified procedure reported earlier in literature. ¹H, ³¹P, ¹³C, and VT-NMR spectra were recorded on a Bruker Avance DPX 300 MHz spectrometers, and a Bruker Avance II 400 MHz NMR spectrometer, respectively, operating at 400.13 MHz for ¹H, 121.49 and 161.96 MHz for ³¹P. The chemical shift (δ) and coupling constant (J) are reported in ppm and Hz, respectively. ESI mass spectrum recorded on a Fison Quattro Bio-Q (Fisons Instruments, VG Biotech, U. K.). UV-visible absorption spectra were measured on a Perkin Elmer Lambda 750 spectrophotometer using quartz cells with path length of 1 cm. The photoluminescence excitation and emission spectra were recorded by an Edinburgh FLS920 spectrophotometer with the Xe900 lamp as the excitation source. The photoluminescence at 77 K were recorded in an EPR tube with a Cold Finger Dewars Flask. The photoluminescence decays were measured by using an Edinburgh FLS920 spectrometer with a gated hydrogen arc lamp using a scatter solution to profile the instrument response function. X-ray Photoelectron spectroscopy (XPS) spectrum was recorded by using a PHI 5000 VersaProbe-Scanning ESCA Microprobe. Melting points were measured by using a Fargo MP-2D melting point apparatus. The elemental analysis (C, H, and S content) of the sample was determined by Elementar UNICUBE elemental analyzer.

Synthesis of Ag₁₀{S₂P(O^{*i*}Pr)₂}₈, **1**

Method A: Ag₇(H){S₂P(O^{*i*}Pr)₂}₆ (0.050 g, 0.025 mmol) was dissolved in THF (50 mL) and kept stirring in light under N₂ gas at 60 °C for 36h. The colorless solution is gradually changed to red violet. It is dried under vacuum, and Ag₁₀{S₂P(O^{*i*}Pr)₂}₈ can be isolated by thin-layer chromatography using a mixed solvent of CH₂Cl₂ and *n*-hexane (1:1, v/v). The red violet spot (R_f ~ 0.45) on the TLC plate was scraped off and

acetone was used to dissolve the isolated compound, which solution is further filtrated and dried to yield $\text{Ag}_{10}\{\text{S}_2\text{P}(\text{O}^i\text{Pr})_2\}_8$ (0.0145 g, yield: 42.4%, based on Ag).

Method B: $\text{Ag}_7(\text{H})\{\text{S}_2\text{P}(\text{O}^i\text{Pr})_2\}_6$ (0.067 g, 0.032 mmol) and $\text{Ag}_6\{\text{S}_2\text{P}(\text{O}^i\text{Pr})_2\}_6$ (0.0316 g, 0.016 mmol) were dissolved in THF (50 mL), and kept stirring in light under N_2 gas at 60 °C for one day. The colorless solution is gradually changed to red violet. It is dried under vacuum, and $\text{Ag}_{10}\{\text{S}_2\text{P}(\text{O}^i\text{Pr})_2\}_8$ can be isolated by thin-layer chromatography using a mixed solvent of CH_2Cl_2 and *n*-hexane (1:1, v/v). The red violet spot ($R_f \sim 0.45$) on the TLC plate was scraped off and acetone was used to dissolved the isolated compound, which the solution is further filtrated and dried to yield $\text{Ag}_{10}\{\text{S}_2\text{P}(\text{O}^i\text{Pr})_2\}_8$ (0.047 g, yield: 52.8%, based on Ag). $^{31}\text{P}\{^1\text{H}\}$ NMR (161.96 MHz, d_6 -acetone, δ , ppm): 104.5 (7P, S_2P), 105.4 (1P, S_2P) ^1H NMR (400.13 MHz, d_6 -acetone, δ , ppm): 1.37 (d, $^3J_{\text{HH}} = 6$ Hz, 96H, CH_3), 4.92 (m, 16H, CH). M.p.: 172°C. Anal. calcd. for $\text{C}_{48}\text{H}_{112}\text{Ag}_{10}\text{O}_{16}\text{P}_8\text{S}_{16}$: C, 20.70; H, 4.05; S, 18.42. Found: C, 20.37; H, 4.07; S, 18.36.

X-ray Crystallography

Single crystals suitable for X-ray diffraction analysis of **1** were obtained by slow evaporation of methanol solution in dark at room temperature within a week. The single crystals were mounted on the tip of glass fiber coated in paratone oil and then transferred into the cold N_2 gas stream. Data were collected on a Bruker APEX II CCD diffractometer using graphite monochromated Mo $K\alpha$ radiation ($\lambda = 0.71073$ Å) at 100K. Absorption corrections for area detector were performed with SADABS^{S4} and the integration of raw data frame was performed with SAINT.^{S5} The structure was solved by direct methods and refined by least-squares against F^2 using the SHELXL-2018/3 package,^{S6} incorporated in SHELXTL/PC V6.14.^{S7} All non-hydrogen atoms were refined anisotropically. P9, S17, S18, and Ag20 were split into two positions with occupancy ratio 0.7:0.3. The co-crystallized methanol was disordered at two positions with equal occupancy. The residual electron densities of the potential disordered solvent molecules in the solvent accessible region were removed by SQUEEZE procedure, incorporated in PLATON program.^{S8} CCDC 2054938 (**1**) contains the supplementary crystallographic data for compounds **1** in this article. These data can be obtained free of charge from The Cambridge Crystallographic Data Centre via www.ccdc.cam.ac.uk/data_request/cif.

Measurement Quantum Yield

The quantum yield of **1** was determined by a comparative method. Absolute values are calculated by using $[\text{Ru}(\text{bpy})_3]^{2+}$ as the standard sample according to the following equation:

$$\Phi_a = \frac{\frac{F_a}{A_a} \times \eta_a^2}{\frac{F_s}{A_s} \times \eta_s^2} \times \Phi_s$$

Where the subscripts “s” and “a” denote standard and analyte respectively, Φ is the fluorescence quantum yield, F is the integrated fluorescence intensity, A is the absorbance, and η is the refractive index of the solvent.

The standard sample and compound **1** were measured two times, respectively. The experimental parameters are listed in the following table.

	solvent	Absorbance (A)	Integrated fluorescence intensity (F)	F/A (*10 ⁸)	avg. F/A (*10 ⁸)	Quantum Yield (Φ)
standard	H ₂ O	0.0971	6.78E+7	6.98	6.91	0.040 ^{S9}
standard	H ₂ O	0.0974	6.65E+7	6.83		
1	2-MeTHF	0.0645	5.97E+7	9.26	9.34	0.060
1	2-MeTHF	0.0636	5.99E+7	9.42		

Computational Detail

Geometry optimizations were performed by density functional theory (DFT) calculations with the Gaussian 16 package,^{S10} using the BP86 functional^{S10} together with Grimme’s empirical DFT-D3 corrections^{S12} and the Def2-TZVP basis set from EMSL Basis Set Exchange Library.^{S13} All the optimized geometries were characterized as true minima by vibrational analysis. The NAO charges and Wiberg bond indices were computed with the NBO 6.0 program^{S14} The UV-visible transitions were calculated by means of time-dependent DFT (TD-DFT) calculations, in which only singlet-singlet transitions were considered. Using the BP86 functional led to a simulated spectrum red-shifted with respect to the experimental one. Using a hybrid functional such as B3LYP^{S15} on the same geometry yielded a similar shape, but this time with a very good agreement with the experimentally recorded λ_{max} . Thus we report here the results obtained with the B3LYP functional. The UV-visible spectra were simulated from the computed TD-DFT transitions and their oscillator strengths by using the SWizard program,^{S16} each transition is associated with a Gaussian function of half-

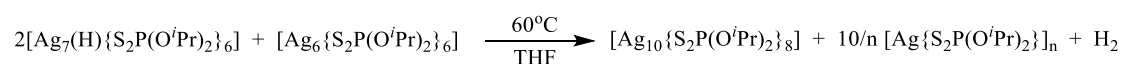
height width equal to 2000 cm⁻¹. The compositions of the molecular orbitals were calculated using the AOMix program.^{S17}

References

- S1. Perrin, D. D.; Armarego, W. L. F. Purification of laboratory chemicals. 4th Edition, Butterworth Heinemann Press, Oxford, 1996.
- S2. Liu, C. W.; Lin, Y.-R.; Fang, C.-S.; Latouche, C.; Kahlal, S.; Saillard, J.-Y. *Inorg. Chem.* **2013**, *52*, 2070-2077.
- S3. Liu, C. W.; Pitts, J. T.; Fackler Jr., J. P. *Polyhedron* **1997**, *16*, 3899-3909.
- S4. SADABS, version 2014-11.0, Bruker Area Detector Absorption Corrections, Bruker AXS Inc., Madison, WI, 2014.
- S5. SAINT, V8.30A, Software for the CCD detector system, Bruker Analytical: Madison, WI, 2012.
- S6. Sheldrick, G. M. *Acta Cryst. A* **2008**, *64*, 112.
- S7. SHELXTL, version 6.14, Bruker AXS Inc., Madison, Wisconsin, USA, 2003.
- S8. Spek, A. L. *Acta Cryst.* **2009**, *D65*, 148-155.
- S9. Suzuki, K.; Kobayashi, A.; Kaneko, S.; Takehira, K.; Yoshihara, T.; Ishida, H.; Shiina, Y.; Oishi, S.; Tobita, S. *Phys. Chem. Chem. Phys.* **2009**, *11*, 9850-9860.
- S10. Gaussian 16, Revision B.01, Frisch, M. J.; Trucks, G. W.; Schlegel, H. B.; Scuseria, G. E.; Robb, M. A.; Cheeseman, J. R.; Scalmani, G.; Barone, V.; Petersson, G. A.; Nakatsuji, H.; Li, X.; Caricato, M.; Marenich, A. V.; Bloino, J.; Janesko, B. G.; Gomperts, R.; Mennucci, B.; Hratchian, H. P.; Ortiz, J. V.; Izmaylov, A. F.; Sonnenberg, J. L.; Williams-Young, D.; Ding, F.; Lipparini, F.; Egidi, F.; Goings, J.; Peng, B.; Petrone, A.; Henderson, T.; Ranasinghe, D.; Zakrzewski, V. G.; Gao, J.; Rega, N.; Zheng, G.; Liang, W.; Hada, M.; Ehara, M.; Toyota, K.; Fukuda, R.; Hasegawa, J.; Ishida, M.; Nakajima, T.; Honda, Y.; Kitao, O.; Nakai, H.; Vreven, T.; Throssell, K.; Montgomery, J. A., Jr.; Peralta, J. E.; Ogliaro, F.; Bearpark, M. J.; Heyd, J. J.; Brothers, E. N.; Kudin, K. N.; Staroverov, V. N.; Keith, T. A.; Kobayashi, R.; Normand, J.; Raghavachari, K.; Rendell, A. P.; Burant, J. C.; Iyengar, S. S.; Tomasi, J.; Cossi, M.; Millam, J. M.; Klene, M.; Adamo, C.; Cammi, R.; Ochterski, J. W.; Martin, R. L.; Morokuma, K.; Farkas, O.; Foresman, J. B.; Fox, D. J. Gaussian, Inc., Wallingford CT, **2016**.
- S11. (a) Becke, A. D. *Phys. Rev. A*, **1988**, *38*, 3098-3100; (b) Perdew, J. P. *Phys. Rev. B*, **1986**, *33*, 8822-8824.
- S12. Gimme, S. *J. Comput. Chem.* **2006**, *27*, 1787-1799.
- S13. (a) Schaefer, A.; Horn, H.; Ahlrichs, R. *J. Chem. Phys.* **1992**, *97*, 2571-2577; (b) Schaefer, A.; Huber, C.; Ahlrichs, R. *J. Chem. Phys.* **1994**, *100*, 5829-5835.
- S14. Glendening, E. D.; Badenhoop, J. K.; Reed, A. E.; Carpenter, J. E.; Bohmann, J.

- A.; Morales, C. M.; Landis, C. R.; Weinhold, F. *NBO 6.0*; Theoretical Chemistry Institute, University of Wisconsin, Madison, WI, **2013**, <http://nbo6.chem.wisc.edu>.
- S15. (a) Becke, A. D. *J. Chem. Phys.* **1993**, *98*, 5648-5652. (b) Lee, C.; Yang, W.; Parr, R. G. *Phys. Rev. B.* **1988**, *37*, 785. (c) P. J. Stephens, F. J. Devlin, C. F. Chabalowski, M. J. Frisch, *J. Phys. Chem.* **1994**, *98*, 11623-11627.
- S16. Gorelsky, S. I. SWizard program, revision 4.5, <http://www.sg-chem.net>.
- S17. Gorelsky, S. I. AOMix program, <http://www.sg-chem.net>.

Scheme S1. The reaction of $\text{Ag}_7(\text{H})\{\text{S}_2\text{P}(\text{O}^i\text{Pr})_2\}_6$ in the presence of $\text{Ag}_6\{\text{S}_2\text{P}(\text{O}^i\text{Pr})_2\}_6$.



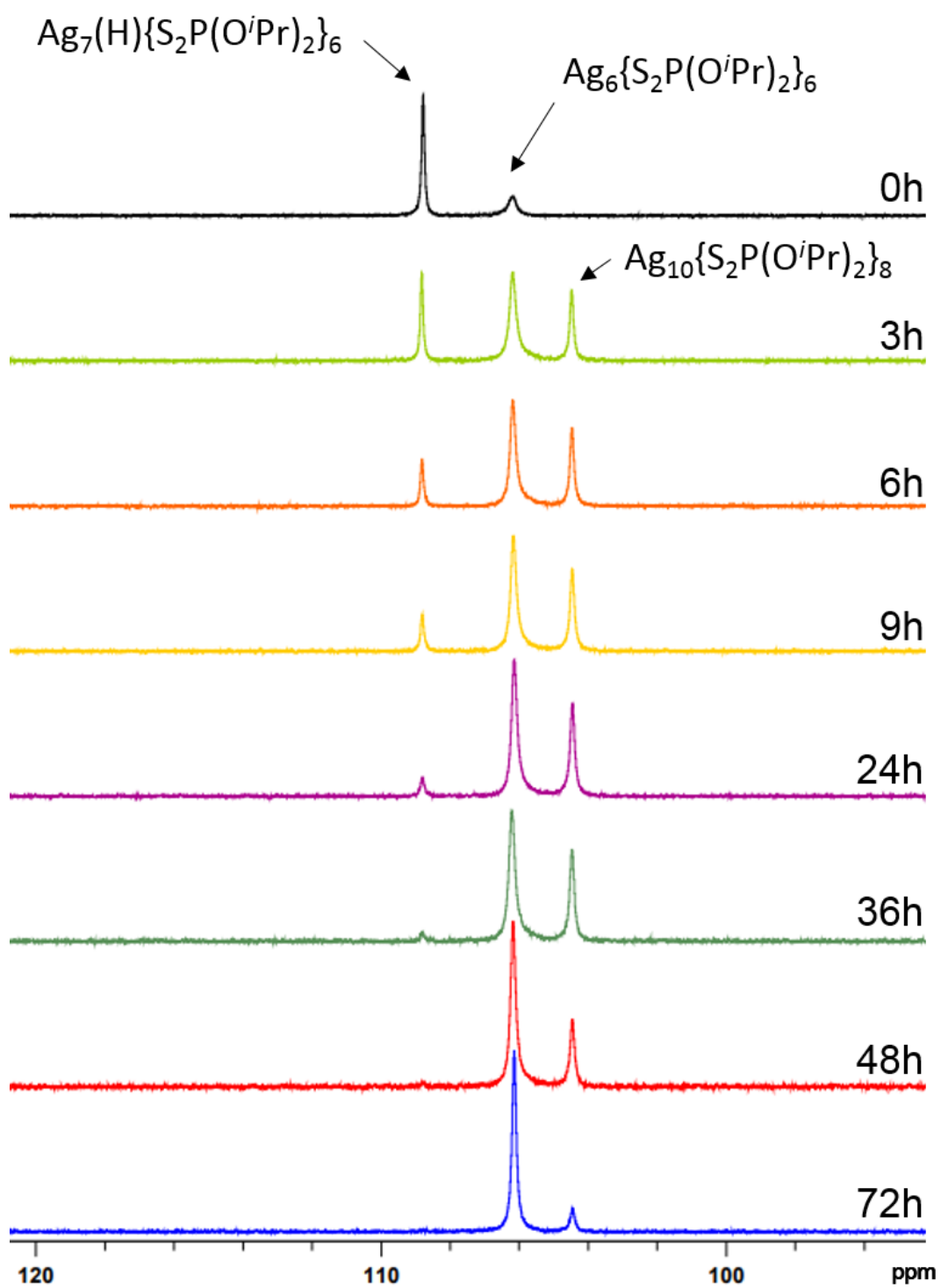


Figure S1. Time-dependent $^{31}\text{P}\{^1\text{H}\}$ NMR spectra of the reaction of $\text{Ag}_7(\text{H})\{\text{S}_2\text{P}(\text{O}^i\text{Pr})_2\}_6$ and $\text{Ag}_6\{\text{S}_2\text{P}(\text{O}^i\text{Pr})_2\}_6$ in a 2:1 molar ratio.

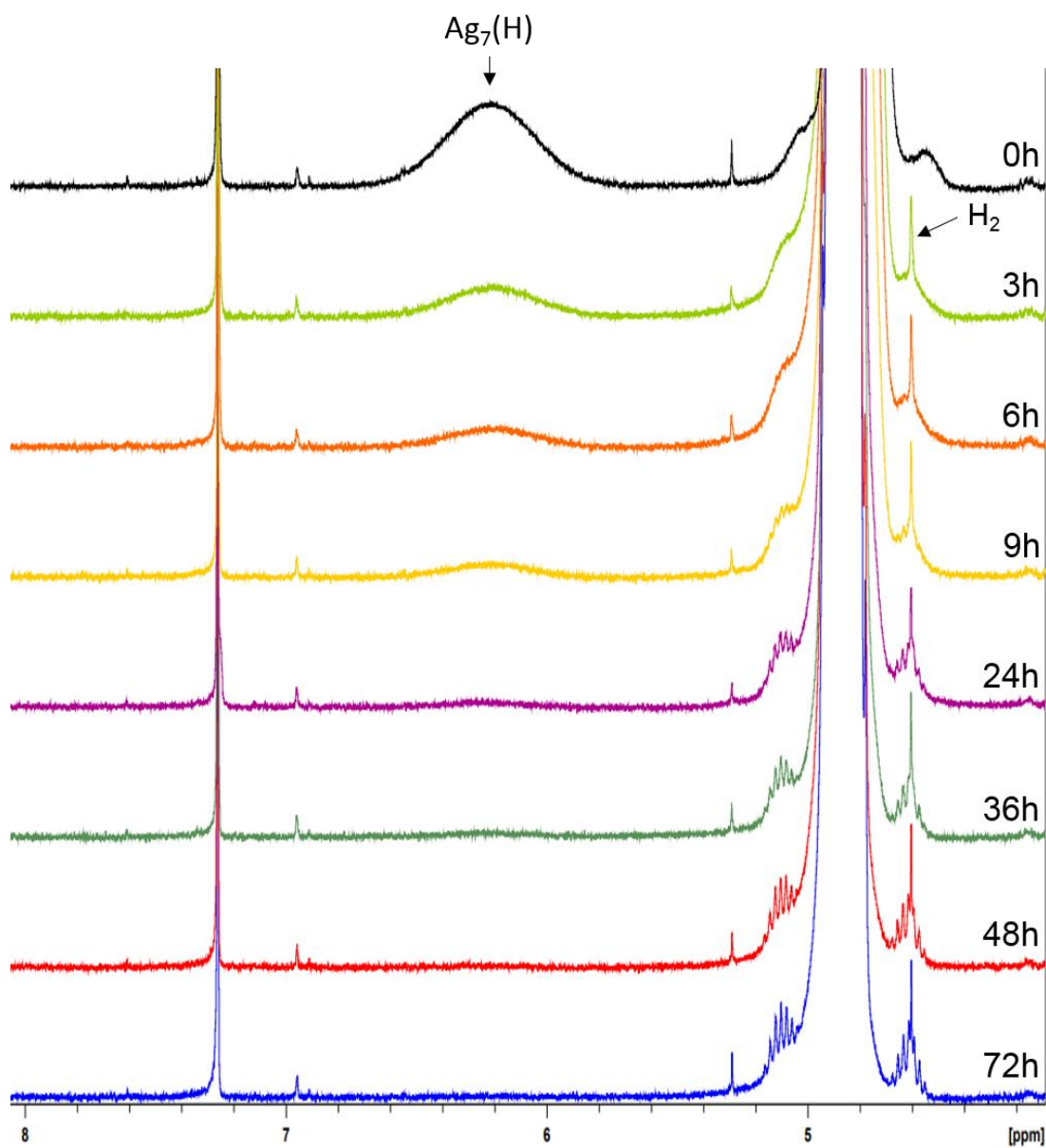


Figure S2. Time-dependent ^1H NMR spectra of the reaction of $\text{Ag}_7(\text{H})\{\text{S}_2\text{P}(\text{O}^i\text{Pr})_2\}_6$ and $\text{Ag}_6\{\text{S}_2\text{P}(\text{O}^i\text{Pr})_2\}_6$ in a 2:1 molar ratio.

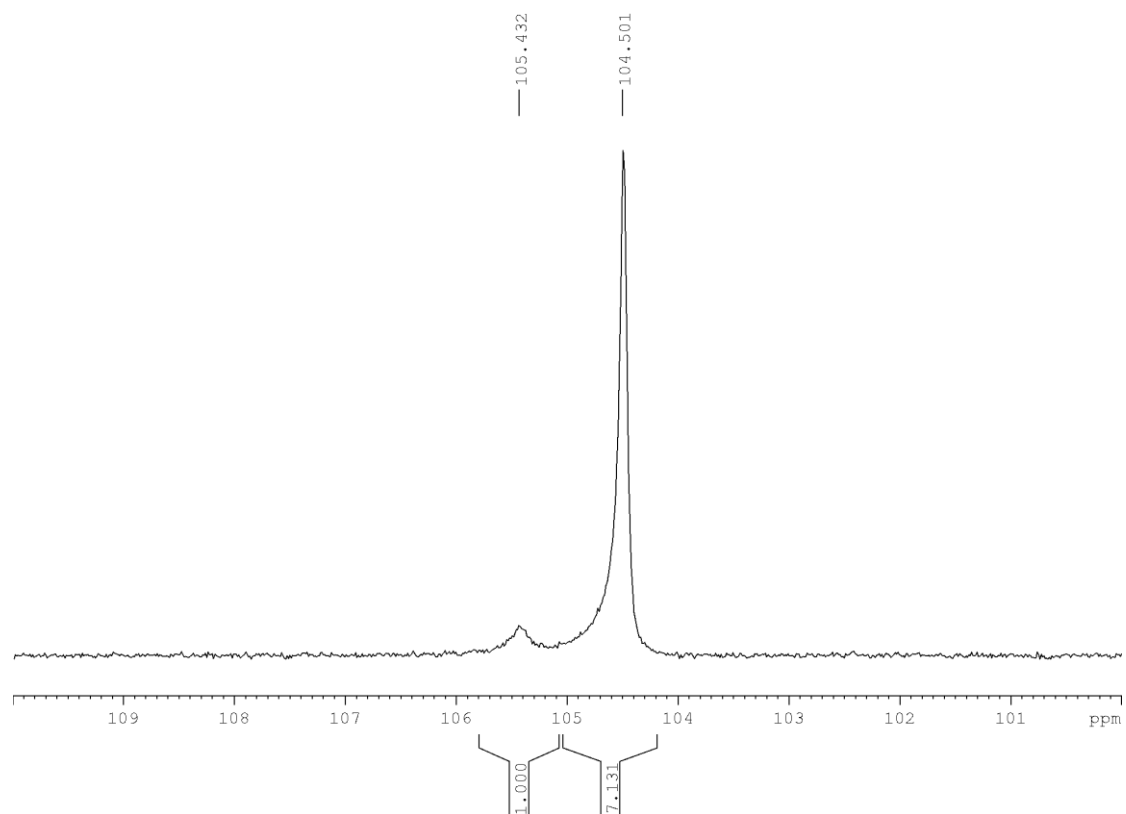


Figure S3. $^{31}\text{P}\{^1\text{H}\}$ NMR (d_6 -acetone) spectrum of **1** at 293K.

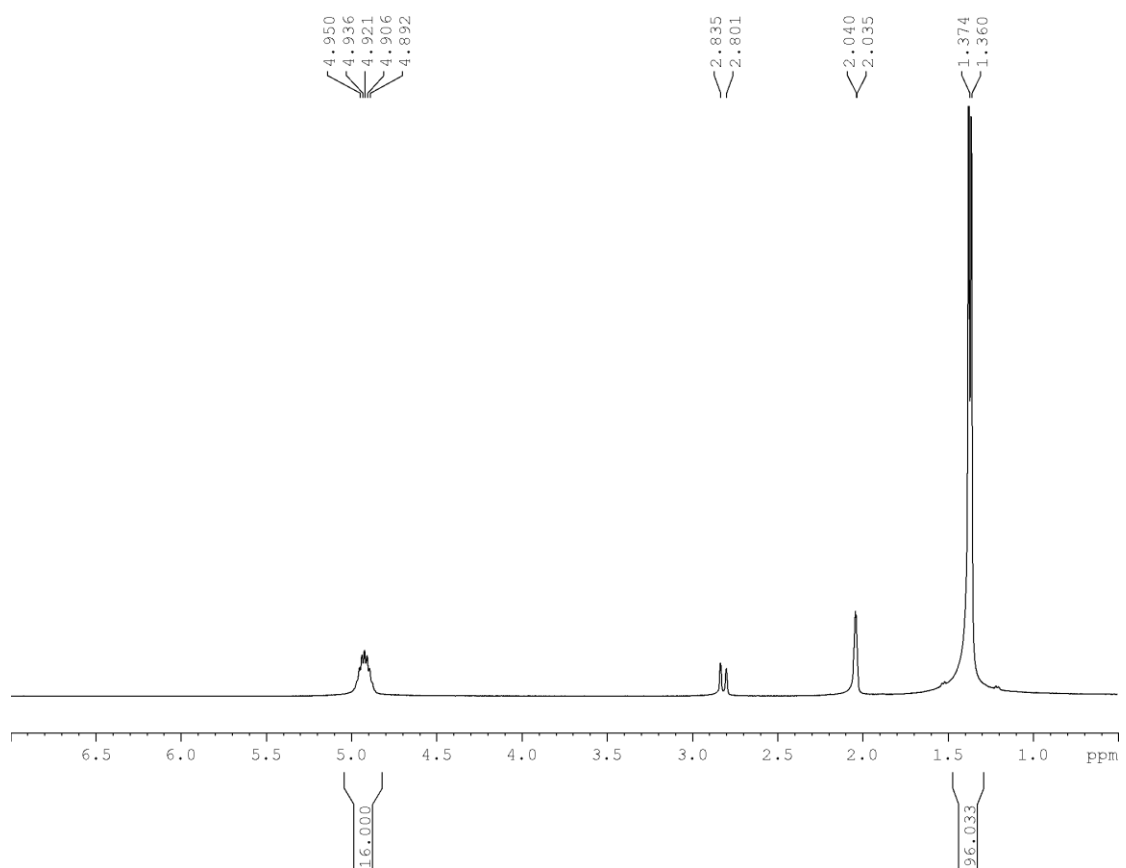


Figure S4. ^1H NMR (d_6 -acetone) spectrum of **1** at 293K.

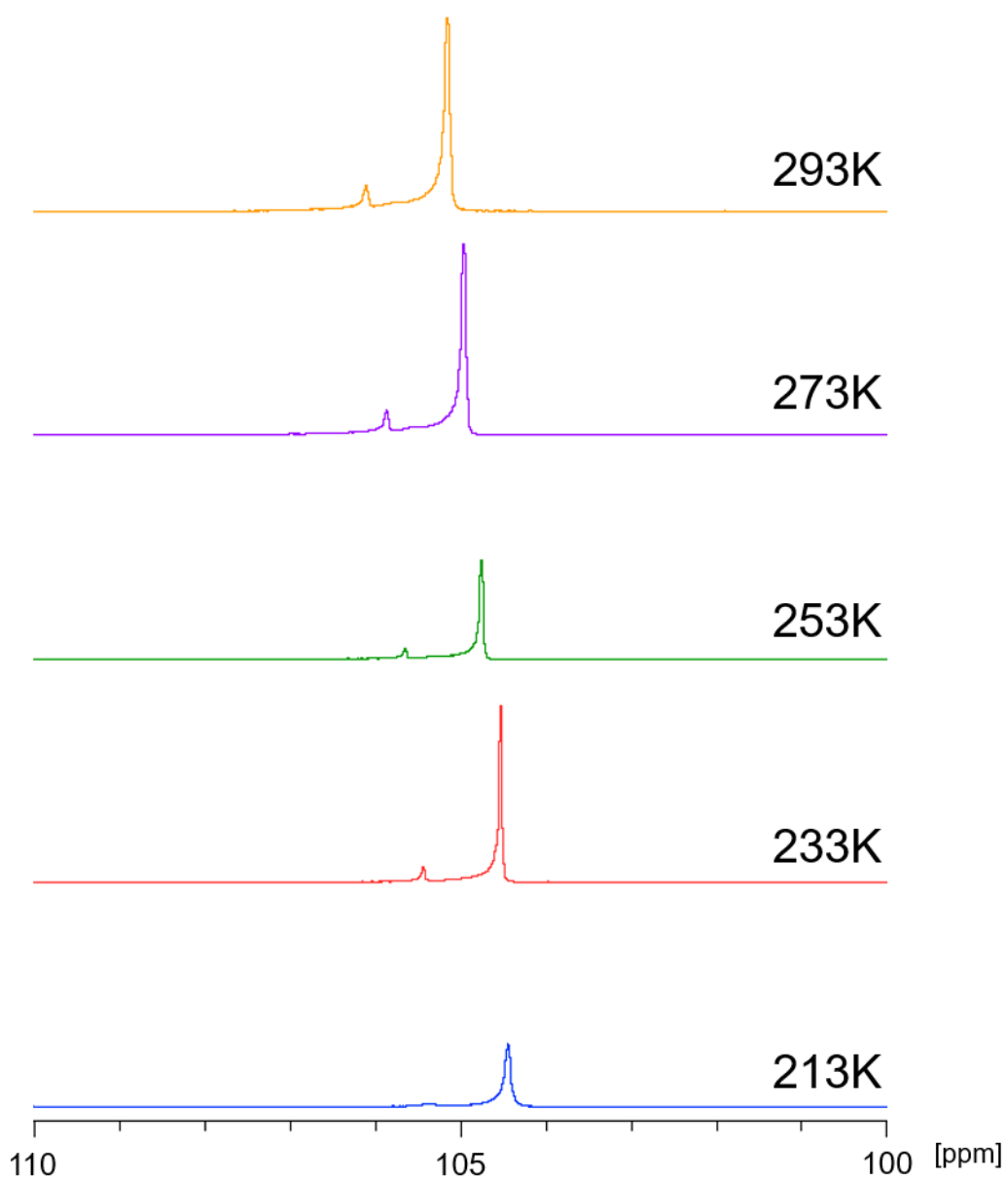


Figure S5. VT $^{31}\text{P}\{^1\text{H}\}$ NMR spectrum (d_6 -acetone) of **1**.

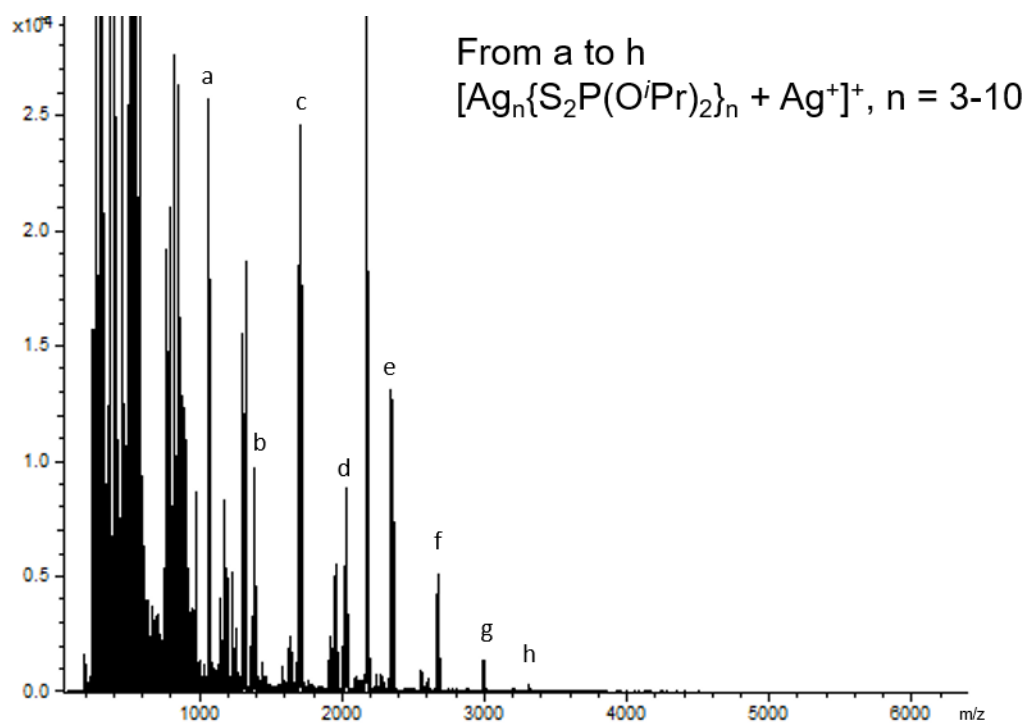


Figure S6. The positive-mode ESI mass spectrum of the product at 106.5 ppm in $^{31}\text{P}\{^1\text{H}\}$ NMR spectrum.

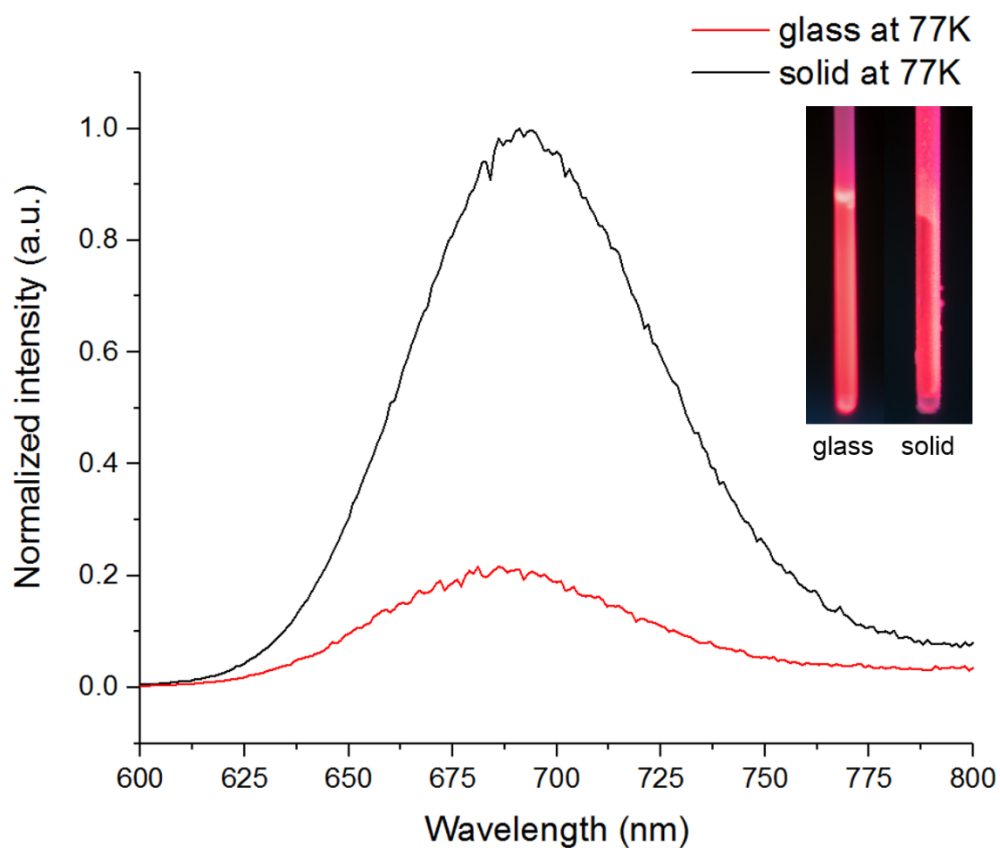


Figure S7. The emission spectrum of **1** in solid and 2-MeTHF glass at 77K

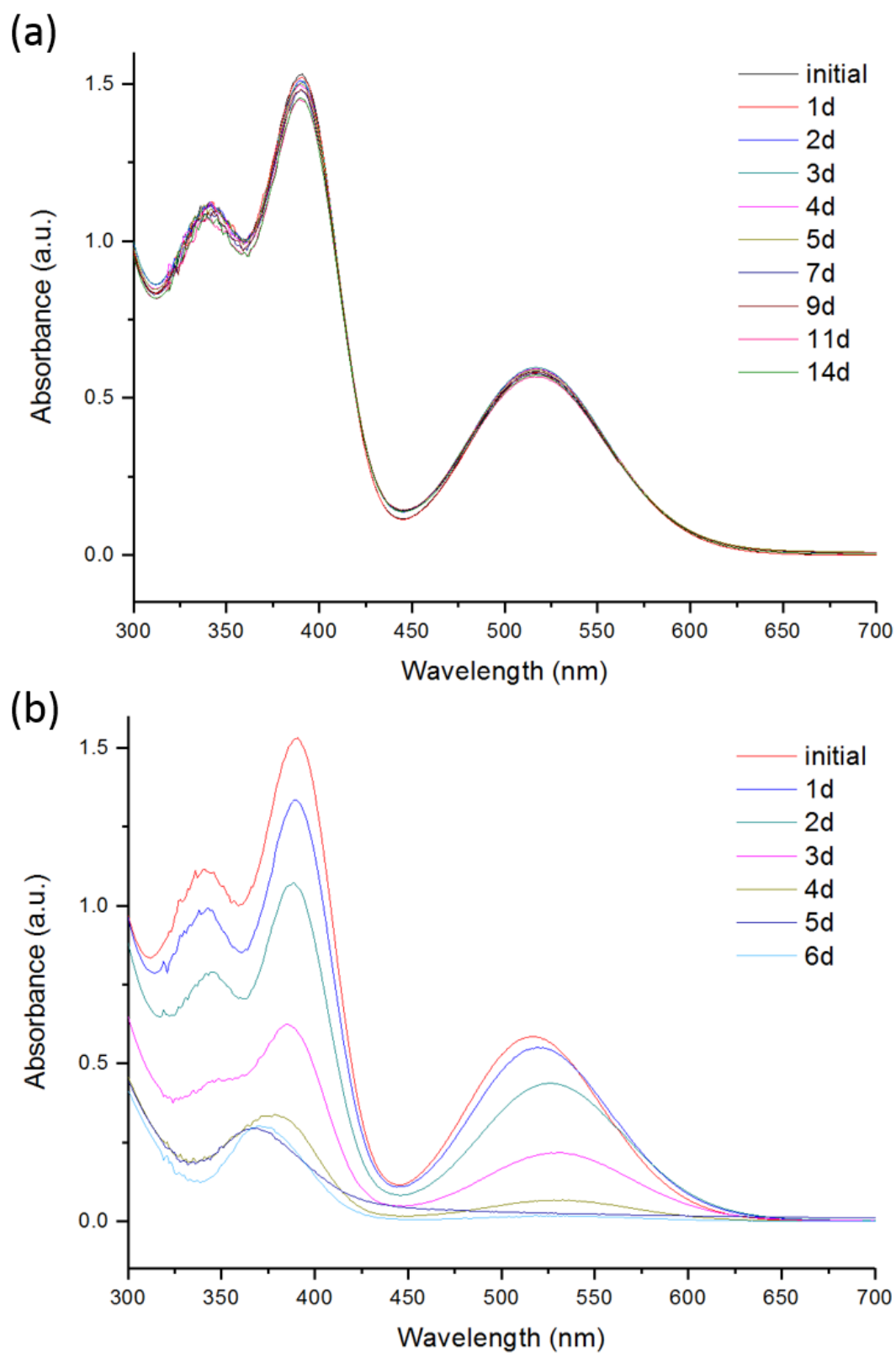


Figure S8. Time-dependent absorption spectrum of **1** (a) in dark and (b) in light.

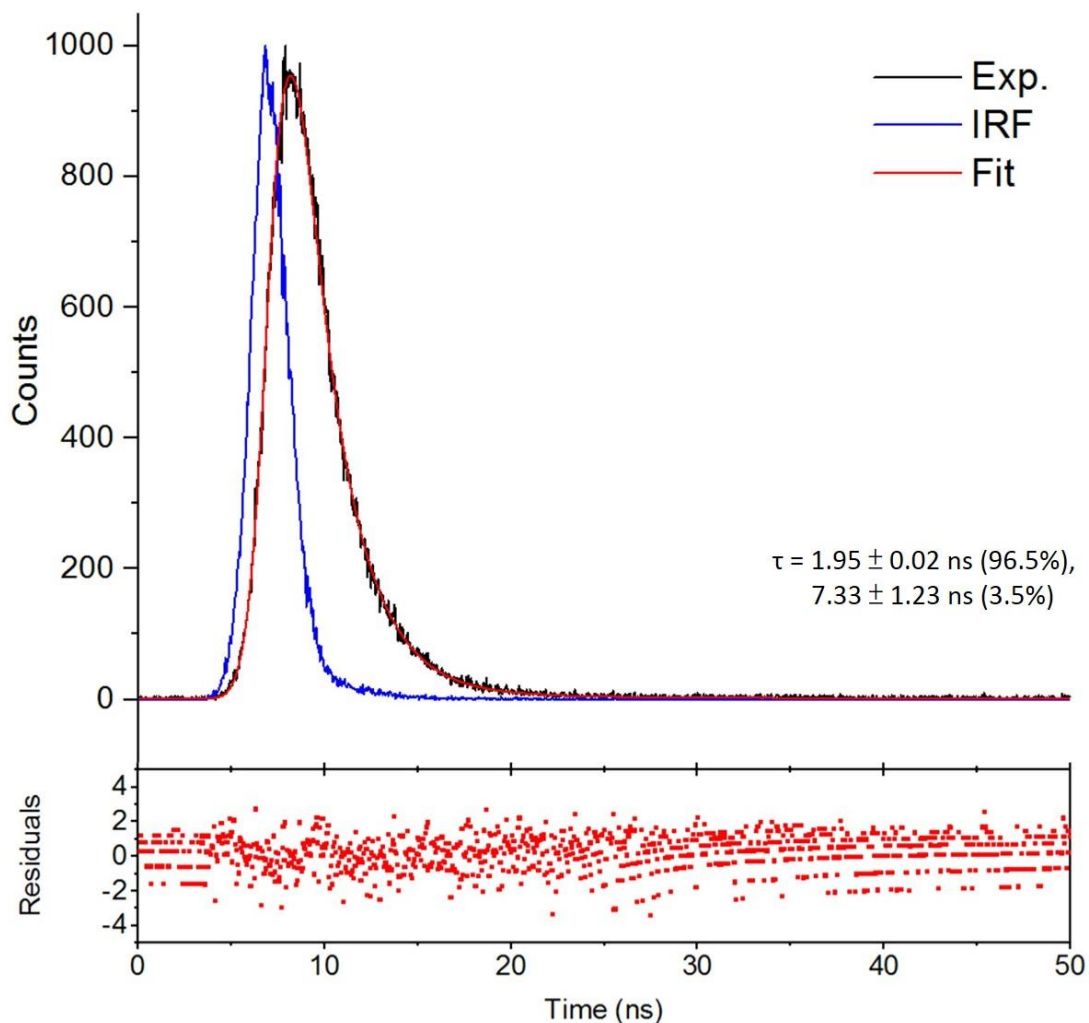


Figure S9. The photoluminescence decay curve of **1** in 2-MeTHF recorded at RT ($\lambda_{\text{ex}} = 520 \text{ nm}$). Fitting Function = $A + B_1 \cdot e^{-t/\tau_1} + B_2 \cdot e^{-t/\tau_2}$, $A = 1.542\text{E}+0$, $B_1 = 4.229\text{E}-2 \pm 2.993\text{E}-4$ (96.5%), $B_2 = 4.070\text{E}-4 \pm 1.487\text{E}-4$ (3.5%), $\tau_1 = 1.950\text{E}-9 \pm 2.233\text{E}-11$, $\tau_2 = 7.325\text{E}-9 \pm 1.229\text{E}-9$.

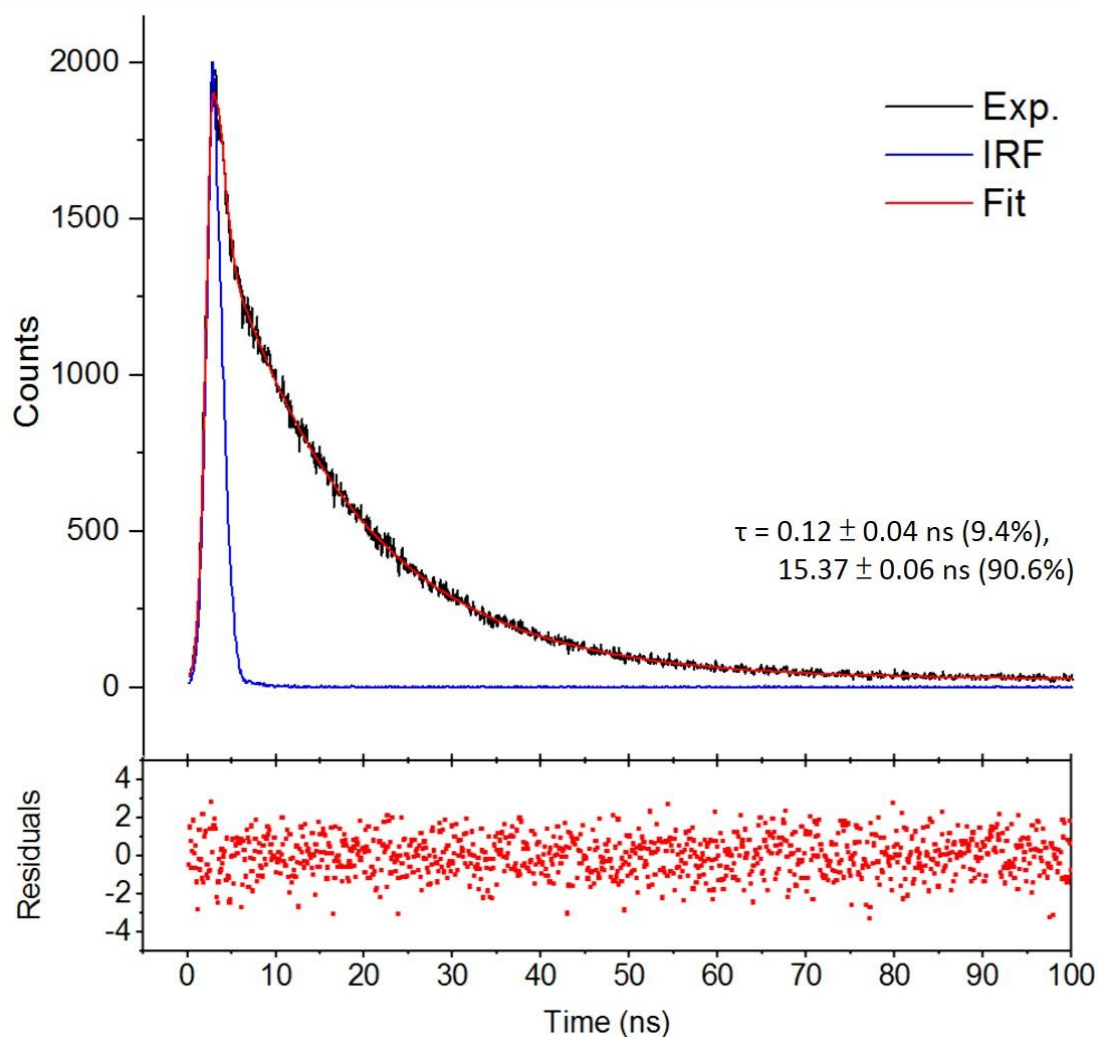


Figure S10. The photoluminescence decay curve of **1** in 2-MeTHF glass recorded at 77 K ($\lambda_{\text{ex}} = 520 \text{ nm}$). Fitting Function = $A + B_1 \cdot e^{-t/\tau_1} + B_2 \cdot e^{-t/\tau_2}$, $A = 1.743\text{E}+1$, $B_1 = 4.419\text{E}-1 \pm 1.467\text{E}-1$ (9.4%), $B_2 = 3.356\text{E}-2 \pm 1.530\text{E}-4$ (90.6%), $\tau_1 = 1.216\text{E}-10 \pm 4.181\text{E}-11$, $\tau_2 = 1.537\text{E}-8 \pm 5.721\text{E}-11$.

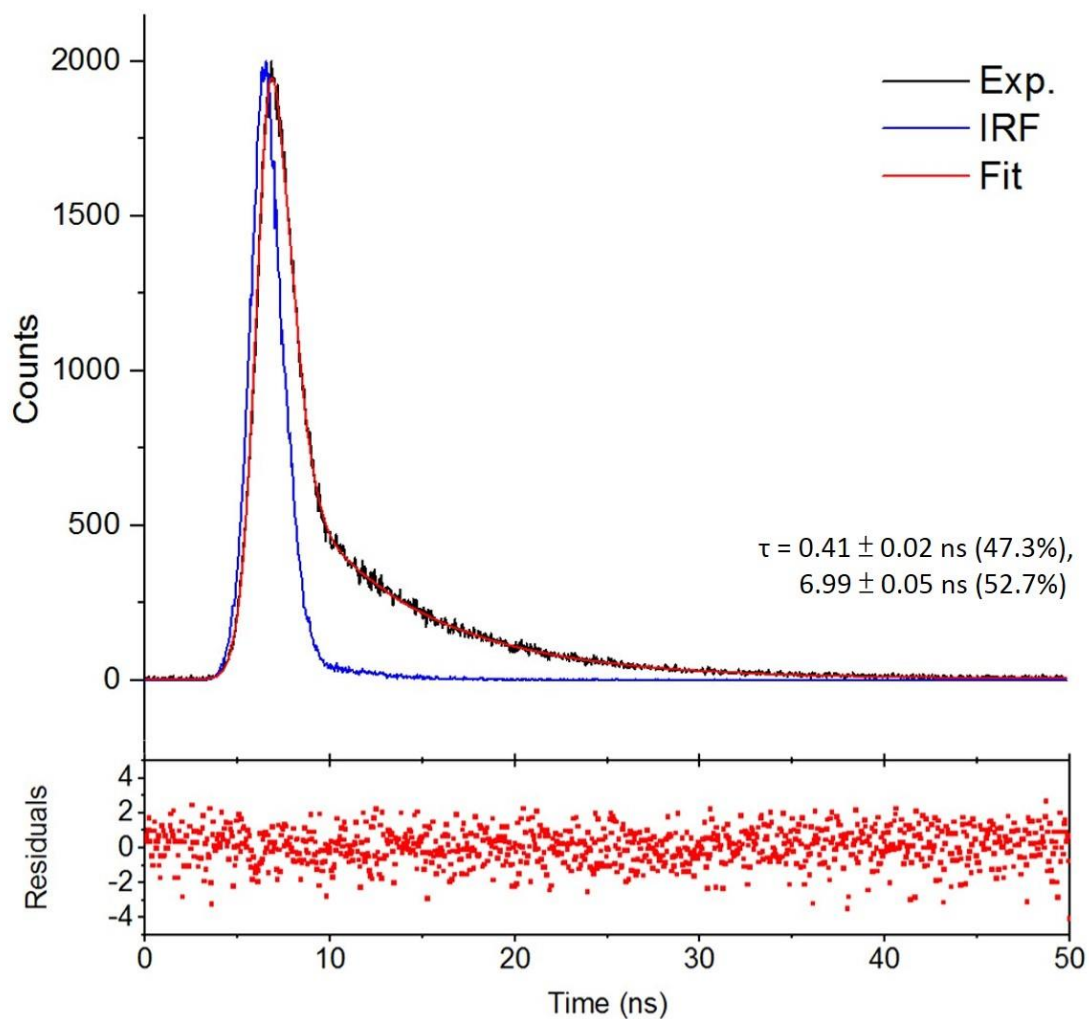


Figure S11. The photoluminescence decay curve of **1** in solid state recorded at RT ($\lambda_{\text{ex}} = 520$ nm). Fitting Function = $A + B_1 \cdot e^{-t/\tau_1} + B_2 \cdot e^{-t/\tau_2}$, $A = 5.889\text{E}+0$, $B_1 = 1.069\text{E}-1 \pm 3.891\text{E}-3$ (47.3%), $B_2 = 6.942\text{E}-3 \pm 6.524\text{E}-5$ (52.7%), $\tau_1 = 4.073\text{E}-10 \pm 1.531\text{E}-11$, $\tau_2 = 6.993\text{E}-9 \pm 4.805\text{E}-11$.

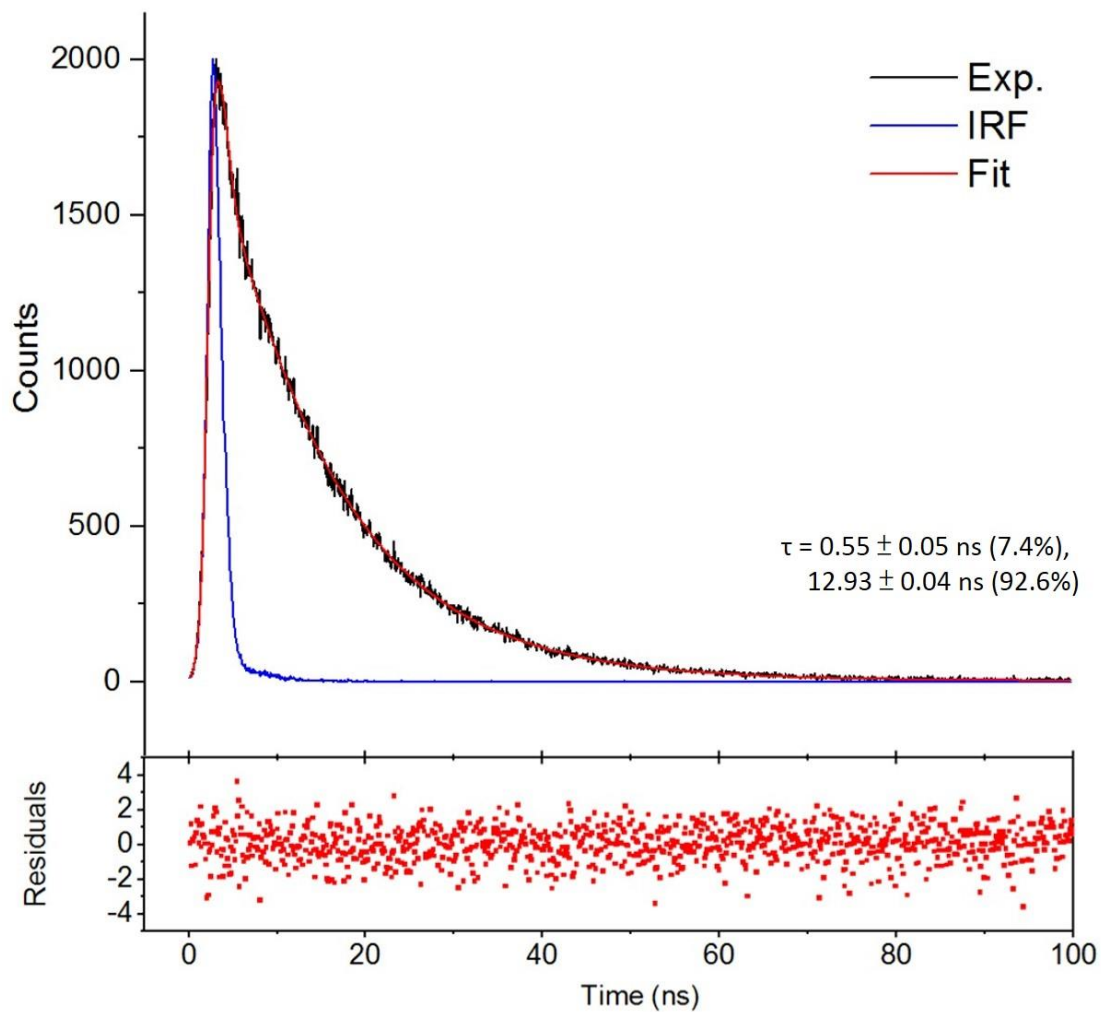


Figure S12. The photoluminescence decay curve of **1** in solid state recorded at 77 K ($\lambda_{\text{ex}} = 520 \text{ nm}$). Fitting Function = $A + B_1 \cdot e^{(-t/\tau_1)} + B_2 \cdot e^{(-t/\tau_2)}$, $A = 4.222\text{E}+0$, $B_1 = 7.798\text{E}-2 \pm 8.102\text{E}-3$ (7.4%), $B_2 = 4.141\text{E}-2 \pm 1.753\text{E}-4$ (92.6%), $\tau_1 = 5.506\text{E}-10 \pm 5.270\text{E}-11$, $\tau_2 = 1.293\text{E}-8 \pm 4.114\text{E}-11$.

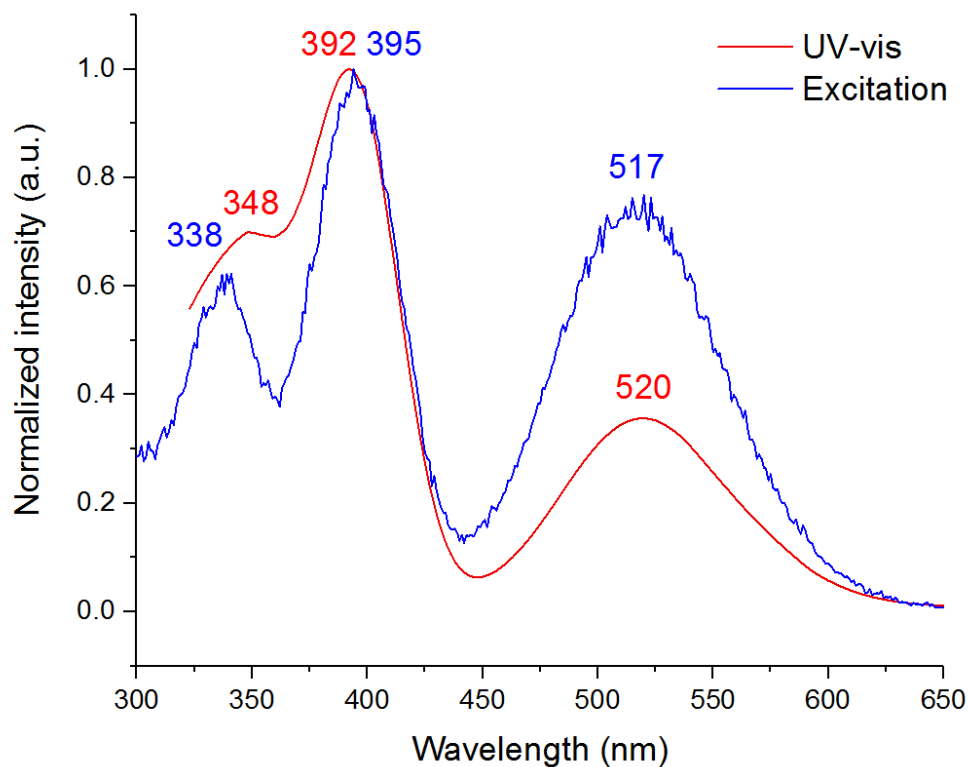


Figure S13. The UV-vis absorption (red line) and excitation spectra (blue line) of **1** in 2-MeTHF at RT.

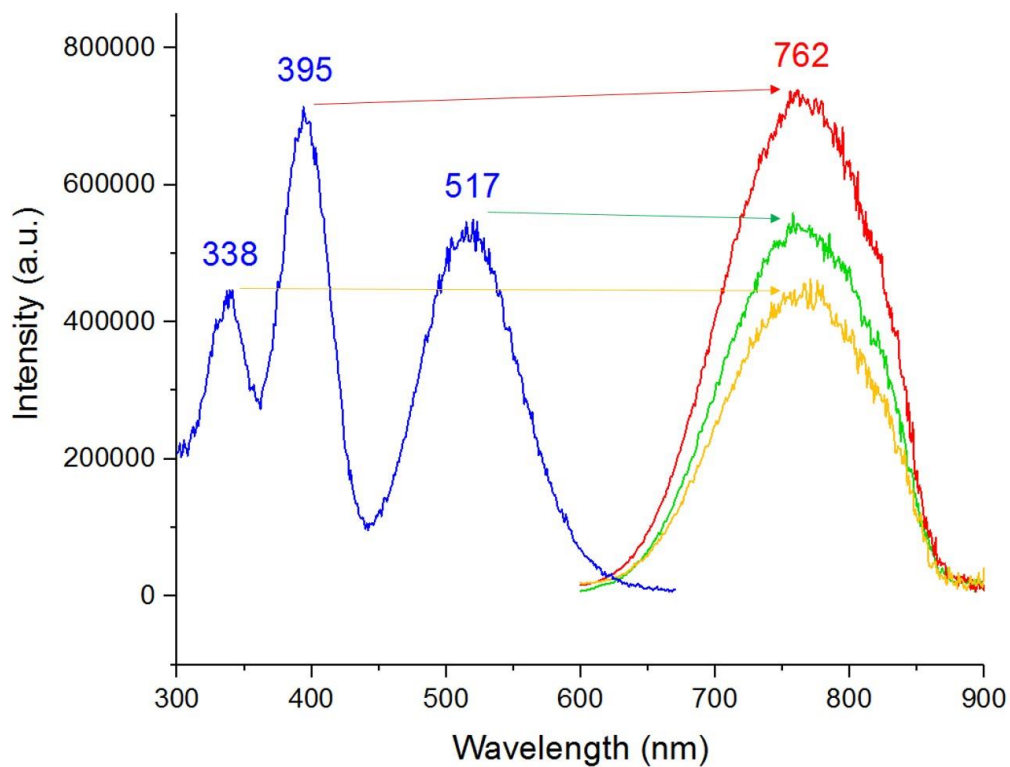


Figure S14. The excitation (blue) and emission spectra of **1** in 2-MeTHF at RT. The emission spectra were excited at 338 (yellow), 395 (green), and 517 nm (red), respectively.

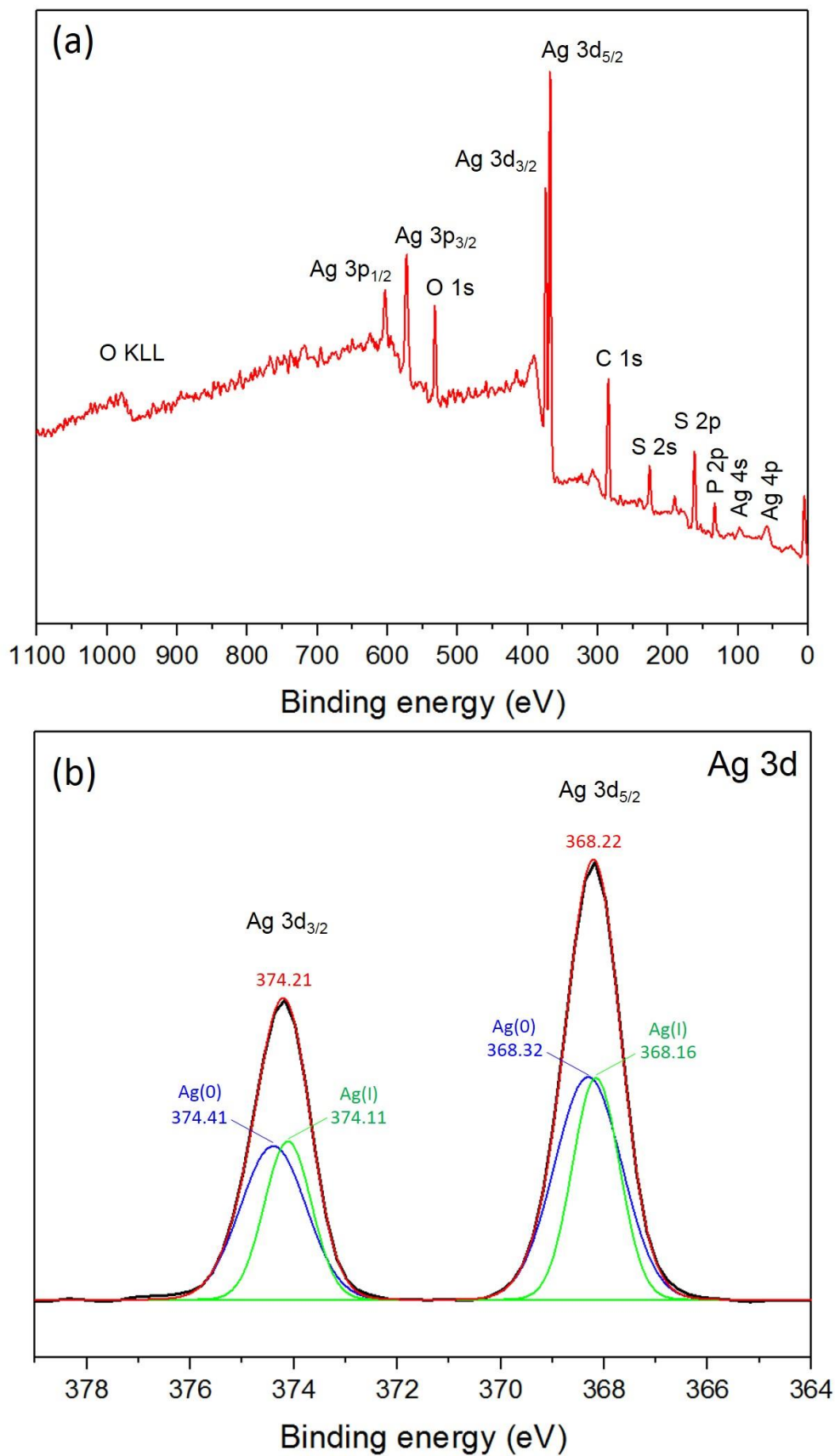


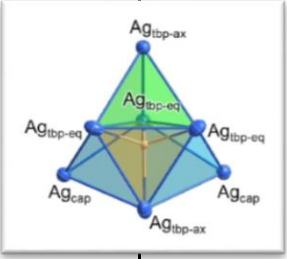
Figure S15. (a) The full and (b) Ag 3d XPS spectrum of **1**.

Table S1. The known 2-e silver NCs and the structure type of their metal core.

Compound	Core structure type	Reducing agent	Ref.
Ag ₁₄ (SC ₆ H ₃ F ₂) ₁₂ (PPh ₃) ₈	[Ag ₆] ⁴⁺ octahedron	NaBH ₄	a
[Ag ₁₄ (C ₂ B ₁₀ H ₁₀ S ₂) ₆ (CH ₃ CN) ₈]·4CH ₃ CN	[Ag ₆] ⁴⁺ octahedron	DMF	b
[Ag ₁₄ (C ₂ B ₁₀ H ₁₀ S ₂) ₆ (pyridine) ₈]	[Ag ₆] ⁴⁺ octahedron	DMF	b
[Ag ₁₄ (C ₂ B ₁₀ H ₁₀ S ₂) ₆ (p-methylpyridine) ₈]	[Ag ₆] ⁴⁺ octahedron	DMF	b
{[Ag ₁₄ (C ₂ B ₁₀ H ₁₀ S ₂) ₆ (Pyrazine) _{6.5} (DMAc)(CH ₃ CN) _{0.5}]·2DMAc} _n	[Ag ₆] ⁴⁺ octahedron	DMF	b
{[Ag ₁₄ (C ₂ B ₁₀ H ₁₀ S ₂) ₆ (dpd) ₂ (CH ₃ CN) ₄]·DMAc} _n	[Ag ₆] ⁴⁺ octahedron	DMF	b
{[Ag ₁₄ (C ₂ B ₁₀ H ₁₀ S ₂) ₆ (bpy) ₄] _n	[Ag ₆] ⁴⁺ octahedron	DMF	b
{[Ag ₁₄ (C ₂ B ₁₀ H ₁₀ S ₂) ₆ (dpbz) ₄] _n	[Ag ₆] ⁴⁺ octahedron	DMF	b
(TBA) ₈ [Ag ₆ (γ-H ₂ SiW ₁₀ O ₃₆) ₂]·5H ₂ O	[Ag ₆] ⁴⁺ octahedron	Me ₂ PhSiH	c
[Ag ₆ @(MoO ₄) ₇ @Ag ₅₆ (MoO ₄) ₂ (^t PrS) ₂₈ (p-TOS) ₁₄ (DMF) ₄]	[Ag ₆] ⁴⁺ octahedron	DMF	d
[Ag ₆ @(MoO ₄) ₇ @Ag ₅₆ (MoO ₄) ₂ (^t PrS) ₂₈ (p-TOS) ₁₄ ·3DMF]	[Ag ₆] ⁴⁺ octahedron	DMF	d
[Ag ₆ @(MoO ₄) ₇ @Ag ₅₆ (MoO ₄) ₂ (^t PrS) ₂₈ (CF ₃ SO ₃) ₁₄ (DMF) ₄]	[Ag ₆] ⁴⁺ octahedron	DMF	d
[Ag ₆ @(MoO ₄) ₇ @Ag ₅₆ (MoO ₄) ₂ (^t PrS) ₂₈ (NO ₃) ₁₄]	[Ag ₆] ⁴⁺ octahedron	DMF	d
[Ag ₆ @(MoO ₄) ₇ @Ag ₆₀ (MoO ₄) ₂ (^t PrS) ₂₈ (PhCOO) ₁₈ (CH ₃ OH) ₂]	[Ag ₆] ⁴⁺ octahedron	DMF	e
[Ag ₆ @(MoO ₄) ₇ @Ag ₆₀ (MoO ₄) ₂ (^t BuS) ₂₈ (PhCOO) _{17.5}]·0.5PhCOO	[Ag ₆] ⁴⁺ octahedron	DMF	e
[Ag ₆ @(MoO ₄) ₇ @Ag ₆₀ (MoO ₄) ₂ (^t PrS) ₂₈ (OAc) ₁₆ (CH ₃ OH) ₄]·2OAc	[Ag ₆] ⁴⁺ octahedron	DMF	e
[Ag ₆ @(CrO ₄) ₈ @Ag ₅₂ (^t PrS) ₃₀ (DMF) ₁₄]·10BF ₄ ·2DMF	[Ag ₆] ⁴⁺ octahedron	DMF	f
(TBA) ₂ {Ag ₆ Ti ₆ (Sal) _{5.5} (L ₁) ₆ (HL ₁) _{0.5} }·2DMF	[Ag ₆] ⁴⁺ octahedron	DMF	g
(Hdpa) ₂ {Ag ₈ Ti ₄ (Sal) ₁₂ }·2DMF	[Ag ₈] ⁶⁺ tetracapped tetrahedron	DMF	g
(TBA) ₂ {Ag ₈ Ti ₄ (Sal) ₁₂ }·2DMF	[Ag ₈] ⁶⁺ tetracapped tetrahedron	DMF	g
(Ag(2,2'-bipy) ₂)(Ag(2,2'-bipy)(CH ₃ CN)){Ag ₈ Ti ₄ (Sal) ₁₂ }	[Ag ₈] ⁶⁺ tetracapped tetrahedron	DMF	g
(Ag ₂ (2,2'-bipy) ₃ DMF){Ag ₈ Ti ₄ (Sal) ₁₂ }·2DMF	[Ag ₈] ⁶⁺ tetracapped tetrahedron	DMF	g
(Ag(CH ₃ CN) ₃){Ag ₉ Ti ₄ (Sal) ₁₂ (CH ₃ CN) ₃ }	[Ag ₈] ⁶⁺ tetracapped tetrahedron	DMF	g
(Ag(1,10-phen)){Ag ₉ Ti ₄ (Sal) ₁₂ (1,10-phen)(DMF)}·2DMF	[Ag ₈] ⁶⁺ tetracapped tetrahedron	DMF	g
[Ag ₁₉ (dppm) ₃ (PhC≡C) ₁₄](SbF ₆) ₃	[Ag ₁₃] ¹¹⁺ anti-cuboctahedron	NaBH ₄	h
[Ag ₂₅ (dpppe) ₃ (MeO-PhC≡C) ₂₀](SbF ₆) ₃	[Ag ₁₃] ¹¹⁺ anti-cuboctahedron	NaBH ₄	h
{[(CH ₃) ₂ NH ₂] ₆ [Ag ₈ (pfga) ₆]·H ₂ O·6DMF}	[Ag ₈] ⁶⁺ rhombohedron	DMF	i
Ag ₁₆ (DPPE) ₄ (SC ₆ H ₃ F ₂) ₁₄	[Ag ₈] ⁶⁺	NaBH ₄	j
(TBA) ₉ H ₄ [Ag ₇ (Si ₃ W ₂₇ O ₉₆)]·12C ₃ H ₆ O	fcc [Ag ₇] ⁵⁺	H ₂ O ^[1]	k
[Ag ₁₀ {S ₂ P(O ^t Pr) ₂ }] ₈	[Ag ₅] ³⁺ trigonal bipyramid	[Ag ₇ (H){S ₂ P(O ^t Pr) ₂ }] ₆	

DMF = dimethylformamide, DMAc = dimethylacetamide, dpd = dipyridin-4-yl-diazene, bpy = 4,4'-bipyridine, dpbz = 1,4-bis(4-pyridyl)benzene, TBA = tetra-n-butylammonium, p-TOS = p-toluenesulfonate, Sal = salicylic acid, H₃L₁ = 2,6-dihydroxybenzoic acid, dpd = 2,2'-dipyridylamine, bipy = 2,2'-dipyridylamine, 1,10-phen = 1,10-phenanthroline, dppm = bis(diphenylphosphino)methane, dpppe = bis(diphenylphosphanyl)pentane, pfga = perfluoroglutarate, dppe = 1,2-bis(diphenylphosphino)ethane. ^[1] According to the authors. ^a *Chem. Commun.* **2013**, 49, 300-3020; ^b *J. Am. Chem. Soc.* **2018**, 140, 1069-1076; ^c *Chem. Commun.* **2013**, 49, 376-378; ^d *Nat. Commun.* **2018**, 9, 2094; ^e *Chem. Commun.* **2019**, 55, 10296-10299; ^f *Sci. China Chem.* **2020**, 63, 16-20; ^g *Nano Res.* **2020**, DOI: 10.1007/s12274-020-3227-5; ^h *Nanoscale* **2017**, 9, 11405-11409; ⁱ *J. Am. Chem. Soc.* **2020**, 142, 16905-16909; ^j *Nanoscale* **2013**, 5, 2674-2677; ^k *Angew. Chem. Int. Ed.* **2020**, 59, 16361-16365.

Table S2. Selected bond lengths in $\text{Ag}_7(\text{H})\{\text{S}_2\text{P}(\text{OEt})_2\}_6$ and **1**.

Compound	Td Edge Yellow (Å)	Td Edge Green (Å)	Td Edge Cyan (Å)	Td Edge Magenta (Å)	Td Height Yellow (Å)	Td Height Green (Å)	Td Height Cyan (Å)	Td Height Magenta (Å)
$\text{Ag}_7(\text{H})\{\text{S}_2\text{P}(\text{OEt})_2\}_6$	3.149(3) ^[1]	2.939(3) ^[1]	2.897(2) ^[2]		2.567 ^[5]	2.303 ^[5]	2.272 ^[6]	
	3.149(3) ^[1]	2.939(3) ^[1]	2.915(3) ^[2]		2.579	2.545	2.523	
	3.149(3) ^[1]	2.939(3) ^[1]	2.922(3) ^[2]		2.579	2.545	2.539	
	3.161(3)	3.161(3)	3.149(3)		2.579	2.545	2.543	
	3.161(3)	3.161(3)	3.149(3)		avg. 2.576	avg. 2.485	avg. 2.469	
	3.161(3)	3.161(3)	3.161(3)				2.272 ^[6]	
	avg. 3.155(3)	avg. 3.050(3)	avg. 3.032(3)				2.523	
			2.897(2) ^[2]				2.539	
			2.915(3) ^[2]				2.543	
			2.922(3) ^[2]				avg. 2.469	
			3.149(3)				avg. 2.469 ^[9]	
			3.149(3)					
		3.161(3)						
		avg. 3.032(3)						
		avg. 3.032(3) ^[3]						
$\text{Ag}_{10}\{\text{S}_2\text{P}(\text{OEt})_2\}_8$	2.7985(13) ^[1]	2.7848(14) ^[1]	2.8437(14)	2.9116(14) ^[4]	2.283	2.276	2.334	2.353 ^[8]
	2.8369(13)	2.8369(13)	2.8549(12)	3.0570(13) ^[4]	2.313	2.339	2.382	2.400
	2.8437(14) ^[1]	2.8464(12)	2.9567(13)	3.0967(15) ^[4]	2.344 ^[5]	2.343 ^[5]	2.402	2.688
	2.8464(12)	2.8549(12)	3.0290(13) ^[2]	3.0984(14)	2.377	2.360	2.548 ^[6]	2.731
	2.8549(12)	2.8896(13) ^[1]	3.0483(13) ^[2]	3.1355(13)	avg. 2.329	avg. 2.330	avg. 2.417	avg. 2.543
	2.9567(13) ^[1]	2.9192(13) ^[1]	3.0557(13) ^[2]	3.600(1)			2.347	
	avg. 2.8562(13)	avg. 2.8553(13)	avg. 2.9647(13)	avg. 3.150(1)			2.351	
			2.8549(12)				2.418	
			2.8896(13)				2.530 ^[6]	
			2.9192(13)				avg. 2.412	
			2.9565(13) ^[2]				2.283	
			3.0193(14) ^[2]				2.356	
			3.1315(15) ^[2]				2.376	
			avg. 2.9618(13)				2.437 ^[6]	
			2.7985(13)				avg. 2.363	
			2.8366(13) ^[2]				2.309	
			2.8464(12)				2.340	
			2.9518(15) ^[2]				2.389	
		2.9567(13)				2.577 ^[6]		
		3.0984(14) ^[2]				avg. 2.404		
		avg. 2.9147(13)				avg. 2.399 ^[7]		
		2.7848(14)						
		2.8464(12)						
		2.9192(13)						
		2.9849(14) ^[2]						
		3.0685(14) ^[2]						
		3.1355(13) ^[2]						
		avg. 2.9566(13)						
		avg. 2.9495(13) ^[3]						

Colored background represents the average bond distances. ^[1] Text in bold style represents $\text{Ag}_{\text{tbp-ax}}-\text{Ag}_{\text{tbp-eq}}$ distances. ^[2] $\text{Ag}_{\text{cap}}-\text{Ag}_{\text{tbp-eq}}$ and $\text{Ag}_{\text{cap}}-\text{Ag}_{\text{tbp-ax}}$ distances. ^[3] The average bond length of all cyan tetrahedrons. ^[4] $\text{Ag}_{\text{ext}}-\text{Ag}_{\text{cap}}$ and $\text{Ag}_{\text{ext}}-\text{Ag}_{\text{tbp-eq}}$ distances. ^[5] Distances from Ag_{ax} to $\Delta\text{Ag}_{\text{tbp-eq}}-\text{Ag}_{\text{tbp-eq}}-\text{Ag}_{\text{tbp-eq}}$. ^[6] Distances from Ag_{cap} to $\Delta\text{Ag}_{\text{tbp-ax}}-\text{Ag}_{\text{tbp-eq}}-\text{Ag}_{\text{tbp-eq}}$. ^[7] The average height of all cyan tetrahedrons. ^[8] Distances from Ag_{ext} to $\Delta\text{Ag}_{\text{tbp-eq}}-\text{Ag}_{\text{cap}}-\text{Ag}_{\text{cap}}$.

Table S3. The distribution of $[\text{Ag}_n\{\text{S}_2\text{P}(\text{O}^i\text{Pr})_2\}_n + \text{Ag}^+]^+$, $n = 3-10$ in Figure S6.

Molecular ion	Exp. (m/z)	Calc. (m/z)
$[\text{Ag}_3\{\text{S}_2\text{P}(\text{O}^i\text{Pr})_2\}_3 + \text{Ag}^+]^+$ (a)	1070.6686	1070.6537
$[\text{Ag}_4\{\text{S}_2\text{P}(\text{O}^i\text{Pr})_2\}_4 + \text{Ag}^+]^+$ (b)	1392.5884	1392.6054
$[\text{Ag}_5\{\text{S}_2\text{P}(\text{O}^i\text{Pr})_2\}_5 + \text{Ag}^+]^+$ (c)	1712.5074	1712.5269
$[\text{Ag}_6\{\text{S}_2\text{P}(\text{O}^i\text{Pr})_2\}_6 + \text{Ag}^+]^+$ (d)	2034.4279	2034.4439
$[\text{Ag}_7\{\text{S}_2\text{P}(\text{O}^i\text{Pr})_2\}_7 + \text{Ag}^+]^+$ (e)	2354.3471	2354.3564
$[\text{Ag}_8\{\text{S}_2\text{P}(\text{O}^i\text{Pr})_2\}_8 + \text{Ag}^+]^+$ (f)	2676.2643	2676.2864
$[\text{Ag}_9\{\text{S}_2\text{P}(\text{O}^i\text{Pr})_2\}_9 + \text{Ag}^+]^+$ (g)	2998.1807	2998.2267
$[\text{Ag}_{10}\{\text{S}_2\text{P}(\text{O}^i\text{Pr})_2\}_{10} + \text{Ag}^+]^+$ (h)	3318.0839	3318.1504

Table S4. The photophysical data of **1**.

State	Absorbance λ_{abs} (nm), ϵ ($\text{M}^{-1}\text{cm}^{-1}$)	Excitation λ_{ex} (nm)	Emission λ_{em} (nm)	Quantum Yield (%)	Lifetime (ns)
Solid, 298K		585	725		0.41±0.02 (47.3%) 6.99±0.05 (52.7%)
Solution, 298K	348 (15500), 392 (21300), 520 (8100)	338, 395, 517	762	6.0	1.95±0.02 (96.5%) 7.33±1.23 (3.5%)
Solid, 77K		517	694		0.55±0.05 (7.4%) 12.93±0.04 (92.6%)
Glass, 77K		335, 388, 515	687		0.12±0.04 (9.4 %), 15.37±0.06 (90.6 %)

Table S5. Averaged computed data for **1'** (WBI = Wiberg bond index). Experimental X-ray distances of **1** in brackets for comparison.

Contact	Distance (Å)	WBI
$\text{Ag}_{\text{tbp-eq}}-\text{Ag}_{\text{tbp-eq}}$	2.936 [2.846]	0.171
$\text{Ag}_{\text{tbp-ax}}-\text{Ag}_{\text{tbp-eq}}$	2.949 [2.866]	0.090
$\text{Ag}_{\text{cap}}-\text{Ag}_{\text{tbp}}$	2.958 [2.977]	0.055
$\text{Ag}_{\text{ext}}-\text{Ag}$	3.010 [3.022]	0.036

Table S6. Selected crystallographic data of **1**.

Compound	2[1] \cdot (CH ₃ OH)
CCDC Number	2054938
Chemical formula	C ₉₇ H ₂₂₈ Ag ₂₀ O ₃₃ P ₁₆ S ₃₂
Formula weight	5601.62
Crystal System	Monoclinic
Space group	<i>P</i> 2 ₁ / <i>c</i>
a, Å	24.7391(10)
b, Å	28.6108(11)
c, Å	28.0078(13)
α , deg.	90
β , deg.	98.6950(10)
γ , deg.	90
V, Å ³	19596.2(14)
Z	4
Temperature, K	100(2)
ρ_{calcd} , g/cm ³	1.899
μ , mm ⁻¹	2.472
θ_{max} , deg.	24.999
Completeness, %	99.4
Reflection collected / unique	98982 / 34306 [$R_{\text{int}} = 0.0644$]
Restraints / parameters	630 / 1865
^a R_1 , ^b wR_2 [$I > 2\sigma(I)$]	0.0774, 0.1458
^a R_1 , ^b wR_2 (all data)	0.1128, 0.1581
GOF	1.080
Largest diff. peak and hole, e/Å ³	2.309 and -2.114

^a $R_1 = \frac{\sum ||F_o| - |F_c||}{\sum |F_o|}$. ^b $wR_2 = \{\frac{\sum [w(F_o^2 - F_c^2)^2]}{\sum [w(F_o^2)^2]}\}^{1/2}$.